

# Expansion and correlation dynamics of interacting bosons released from a harmonic trap

Rhombik Roy<sup>1</sup>, Barnali Chakrabarti<sup>1</sup> and Arnaldo Gammal<sup>2</sup>

<sup>1</sup>*Department of Physics, Presidency University, 86/1 College Street, Kolkata 700073, India.*

<sup>2</sup>*Instituto de Física, Universidade de São Paulo, CEP 05580-090, São Paulo, Brazil*

(Dated: November 29, 2022)

We investigate the expansion dynamics of one-dimensional strongly interacting bosons released from a harmonic trap from the first principle. We utilize the multiconfigurational time-dependent Hartree method for bosons (MCTDHB) to solve the many-body Schrödinger equation at high level of accuracy as the MCTDHB basis sets are explicitly time dependent and optimised by variational principle. We probe the expansion dynamics for very strong interaction but not in Tonks-Girardeau (TG) limit and thus integrability breaks down. We characterize the dynamics by measure of expansion radius and expansion velocity. We find that for an wide range of strong interaction strength, the expansion dynamics is trimodal. We present three different time-scales of expansion — inner-core, outer-core and the whole cloud; whereas for non-interacting case, it is unimodal. We also report the dynamics of higher-body densities and correlations and observe the antibunching effect. The two- and three-body densities are characterized by the appearance of correlation hole along the diagonal due to very strong interaction that mimics the Pauli principle. With the expansion of bosons the correlation hole also spread. We also report the expansion dynamics of 1D dipolar bosons released from the trap. When very strong contact interaction leads to fermionization limit, for strongly interacting dipolar bosons lead to crystal phase. The expansion dynamics of dipolar bosons is again trimodal as before, but the expansion velocity is much larger and diverging unlike the case of contact interaction where the expansion velocity is converged. The diverging expansion dynamics is further supported by the unbounded energy for long range interaction.

## I. INTRODUCTION

The non-equilibrium dynamics of isolated strongly correlated many-body systems become the most challenging research area both theoretically and experimentally [1, 2]. The unprecedented control of system parameters in real time in the experiments of ultracold atomic gases makes this field active and draws remarkable interest in recent days [3–7]. It addresses thermalization, particle transportation in the experimental studies of quantum quenches [8–17]. Particle transport is generally classified as either ballistic or diffusive, or a combination of the two [15, 18]. In the ballistic transport, the particles spread out with constant uniform velocity without any signature of non-decaying current. Whereas interaction leads to diffusive type transport specially in higher dimension. However, it is found that during sudden expansion of 1D, two-component Fermi gas into an empty optical lattice, the radius of the cloud grows linearly in time [19]. A very recent work reports the expansion dynamics in a 1D hard-core boson model with three-body interactions, the bosons expand ballistically with weak interaction and the expansion velocity decreases with increase in three-body interaction. One can expect intriguing physics for strongly interacting bosons in reduced dimension. The strongly interacting bosons in the Tonks-Girardeau (TG) limit exhibit an exact mapping to spinless fermions which is an integrable system [2, 20]. In 1D, the hard core bosons in a lattice can also be mapped to non-interacting spinless fermions [21–23]. Several recent studies are also focused to address whether strongly interacting systems will exhibit ballistic or diffusive trans-

port [15, 19, 24–26]. In a recent work we find experimental and numerical investigation of the expansion of localised ultracold bosons in optical lattice [18]. The distribution of the expanding cloud is monitored by standard absorption imaging. It is found that the hard core bosons expand ballistically like the non-interacting fermions. Whereas for the interacting bosons, appearance of diffusive cloud is noted which indicates diffusive dynamics of the centre cloud surrounded by ballistic flow. From the extensive work already published in finding the expansion velocity of the expanding cloud, we find that the physics of expansion dynamics and its time scale is clearly understandable for the hardcore bosonic regime or in the TG limit due to the existence of exact mapping. However, the complexity arises when the bosons are strongly interacting but not in the TG limit and the concept of integrability breaks down, the question of solution of Schrödinger equation from first principle comes in the picture.

In this article, we explore the dynamics from a microscopic general quantum many-body perspective. It requires the complete solution of the time dependent Schrödinger equation. The multi configurational time-dependent Hartree method for bosons (MCTDHB) is used to solve the time dependent Schrödinger equation (TDSE) at a high level of accuracy. The basis sets of MCTDHB are explicitly time-dependent and variationally optimised. We prepare the initial state at the ground state of few interacting bosons in a harmonic oscillator (HO) potential. In the quantum quench, we make the system trapless by a sudden quench from a finite trap frequency to zero. We solve the complete set of equa-

tions (see the numerical method section) with periodic boundary conditions. Thus, the gas is released from a parabolic trap onto a large bath. The time evolution of the expanding cloud consisting of  $N = 4$  bosons is monitored by MCTDHB for several choices of interaction strength parameter ( $\lambda$ ) considering the non-interacting, weakly interacting and strongly interacting limit. The present work is well-suited to a small number of particles because, although such a small number of particles is not typical for experiments in expansion dynamics, it does increase the beyond mean-field effect [27]. Fragmentation of BEC is a mesoscopic effect that decreases with increase in number of particles as  $\frac{1}{\sqrt{N}}$ . Therefore, a lower number of particles is preferable to study the beyond mean-field effect. Also, it is now possible to experiment with small systems [28–31], which gives our system a lot of room for testing.

We find very complex nature of transport mechanisms and three scale of expansion dynamics when the bosons are strongly interacting. The most complex regime is when the bosons are strongly interacting but not in TG limit. We find the density splits into four pieces (equal to number of bosons in the trap) and each piece moves distinctly like an independent jet. Here we find a trimodal dynamics which is associated with expansion of inner core, of outer core and of total cloud. The corresponding expansion velocity also exhibits trimodal distribution. The non-interacting case is unimodal as expected.

As MCTDHB utilises time adaptive basis, the expansion coefficients as well as the orbitals are time dependent, and one can dynamically follow the many-body correlations [32–34]. Using MCTDHB, we can also calculate higher order densities  $\rho^{(p)}$  for  $p = 2, 3$  (two and three-body density), higher order correlation  $g^{(p)}$  for  $p = 2, 3$  (two and three-body correlation). Both  $\rho^{(p)}$  and  $g^{(p)}$  analyze the effect of interaction on the coherence of many-body state during expansion. For strongly interacting bosons, we observe the correlation hole in the higher body densities which occurs due to very strong repulsion between the bosons and mimics the Pauli exclusion principle. With time, the width of the correlation hole increases. For the present calculation, we measure the local two-body and three-body correlation ( $g^{(2)}(0, 0)$ ) and  $g^{(3)}(0, 0, 0)$ ) as a function of time.

We also report the expansion dynamics for four strongly interacting dipolar bosons. The long-range nature of dipolar interaction exhibit variety of interesting phenomena [35–42]. The many-body physics with the cold atoms has also seen triggering consequences of the dipolar interaction [43–48]. For the dipolar interaction, the energy is unbounded with change in interaction strength which is in sharp contrast with contact interaction, where energy is bounded. When the very strong contact interaction leads to fermionization, the same for dipolar interaction leads to crystallization [49]. In our present analysis, we observe dominating effect of the long-range part of the strong dipolar interaction in

the expansion dynamics. The splitted density exhibits diverging feature and the expansion velocity also diverges which is in stark contrast with contact interaction. In the later case, the expansion of four splitted density is converged, the velocity of the whole cloud also converge.

The paper is organised as follows. In Sec. II, we introduce the setup and the necessary theory. Sec. III explains the basic equation used to measure the different quantities. Sec. IV and Sec. V explains our numerical results and explanations. In Sec. VI, we reach our conclusion.

## II. NUMERICAL METHOD

The motivation of the present work is to investigate the expansion and correlation dynamics of strongly interacting bosons both for short-range contact and long-range dipolar interaction, released from a trap. Our investigation is based on the dynamical measures of one-body, two-body and three-body densities as well as their local correlation functions. The key quantity of this calculation is the computation of exact many-body wave function. We solve the full many-body Schrödinger equation for the interacting  $N$ -bosons system by MCTDHB which propagates a given many-body state in time. We are able to solve the time dependent Schrödinger equation at a high level of accuracy. It is demonstrated that MCTDHB can provide exact solutions of time-dependent Schrödinger equation in principle and in practical [50–52].

### A. The many-body wave function

The time dependent Schrödinger equation for  $N$  interacting bosons is given by  $\hat{H}\psi = i\frac{\partial\psi}{\partial t}$ . The total Hamiltonian has the form

$$\hat{H}(x_1, x_2, \dots, x_N) = \sum_{i=1}^N \hat{h}(x_i) + \Theta(t) \sum_{i < j=1}^N \hat{W}(x_i - x_j) \quad (1)$$

The Hamiltonian  $\hat{H}$  is in dimensionless unit which is obtained by dividing the dimensionful Hamiltonian by  $\frac{\hbar^2}{mL^2}$ ,  $m$  is the mass of the bosons,  $L$  is the arbitrary length scale.  $\hat{h}(x) = \hat{T}(x) + \hat{V}(x)$  is the one-body Hamiltonian.  $\hat{T}(x)$  is the kinetic energy operator and  $\hat{V}(x)$  is the external trapping potential.  $\hat{W}(x_i - x_j)$  is the two-body interaction.  $\Theta(t)$  is the Heaviside step function of time  $t$  and implements the quench. The ansatz for the many-body wave function is the linear combination of time dependent permanents

$$|\Psi(t)\rangle = \sum_{\vec{n}} C_{\vec{n}}(t) |\vec{n}; t\rangle, \quad (2)$$

The vector  $\vec{n} = (n_1, n_2, \dots, n_M)$  represents the occupation of the orbitals and  $n_1 + n_2 + \dots + n_M = N$  preserve

the total number of particles. In second quantisation representation, the permanents are given as

$$|\bar{n}; t\rangle = \prod_{i=1}^M \left( \frac{(b_i^\dagger(t))^{n_i}}{\sqrt{n_i!}} \right) |vac\rangle. \quad (3)$$

Distributing  $N$  bosons over  $M$  orbitals, the number of permanents become  $\binom{N+M-1}{N}$ . Thus, if  $M \rightarrow \infty$ , the wave function becomes exact, the set  $|n_1, n_2, \dots, n_M\rangle$  spans the complete  $N$ -particle Hilbert space. Although for practical calculation, we restrict the number of orbitals to the desired value requiring the proper convergence in the measure quantities. It is to be noted that both the expansion coefficients  $\{C_{\bar{n}}(t)\}$  as well as orbitals  $\{\phi_i(x, t)\}_{i=1}^M$  that build up the permanents  $|\bar{n}; t\rangle$  are time dependent and fully variationally optimised quantities. Comparing to time-independent basis, as the permanents are time-dependent, a given degree of accuracy is reached with much shorter expansion [53, 54]. We also emphasise that MCTDHB is more accurate than exact diagonalization which utilises the finite basis and are not optimised. Whereas in MCTDHB, as we use time adaptive many-body basis set, it can dynamically follow the building correlation due to inter-particle interaction [32, 55–57] and it has been widely used in different theoretical calculations [23, 33, 58, 59]. Thus, to obtain the many-body wave function  $|\psi(t)\rangle$ , we evaluate the time dependent coefficients  $\{C_{\bar{n}}(t)\}$  and orbitals  $\{\phi_i(x, t)\}_{i=1}^M$ . We require the stationarity of the action with respect to the variations of the time dependent coefficients and the time dependent orbitals. It results to a coupled set of equations of motion containing  $\{C_{\bar{n}}(t)\}$  and  $\phi_i(x, t)$  which are further solved simultaneously [32, 55, 60–62] by recursive MCTDHB (R-MCTDHB) package [51, 52, 63]. It is to be noted that the one particle function  $\phi_i(x, t)$  and the coefficient  $C_{\bar{n}}(t)$  are variationally optimal with respect to all parameters of the many-body Hamiltonian at any time [64–67]. For the relaxed state we propagate the MCTDHB equations in imaginary time.

### B. System and chosen parameters

In the present work, we consider expansion dynamics of four interacting bosons confined in one-dimensional harmonic oscillator and interacting via contact interaction of strength  $\lambda$  and dipolar interaction strength ( $g_d$ ). Thus, the many-body Hamiltonian becomes

$$\hat{H} = \frac{1}{2} \sum_{i=1}^N \left( -\frac{\partial^2}{\partial x_i^2} + x_i^2 \right) + \sum_{i<j}^N \hat{W}(x_i - x_j) \quad (4)$$

For contact interaction,

$$\hat{W}(x_i - x_j) = \lambda \delta(x_i - x_j) \quad (5)$$

where  $\lambda$  is the interaction strength determined by the scattering length  $a_s$  and the transverse confinement frequency. For long-range dipolar interaction,

$$\hat{W}(x_i - x_j) = \frac{g_d}{|(x_i - x_j)|^3 + \alpha} \quad (6)$$

$g_d$  is the dipolar interaction strength.  $\alpha$  is the short-range cutoff to avoid singularity at  $x_i = x_j$ . We put the cutoff  $\alpha = 0.05$  and checked its consistency by comparing to a long-range interaction augmented with contact potential [41, 68].

Our calculation considers only repulsive interaction:  $\lambda > 0$  and  $g_d > 0$ . Throughout our numerical investigation, we maintain periodic boundary conditions. To study the expansion dynamics, we suddenly switch off the trap and allow the bosons to expand in a large bath. We explicitly present the expansion dynamics for four different choices of interaction strength.  $\lambda = 0$  (non-interacting),  $\lambda = 2$  (weakly interacting),  $\lambda = 5$  (strong interaction) and  $\lambda = 25$  (very strong interaction). For comparison with the case of expansion of long-range dipolar bosons, we choose  $g_d$  in the same range. We fix number of orbitals to  $M = 12$  for converged results.

### III. QUANTITIES OF INTEREST

For the study of expansion dynamics, we employ the following measures:

- (i) The reduced one-body density matrix in coordinate

space is defined as

$$\rho^{(1)}(x'_1|x_1; t) = N \int dx_2 dx_3 \dots dx_N \psi^*(x'_1, x_2, \dots, x_N; t) \psi(x_1, x_2, \dots, x_N; t). \quad (7)$$

Its diagonal gives the one-body density  $\rho(x, t)$  defined as

$$\rho(x; t) = \rho^{(1)}(x'_1 = x|x_1 = x; t) \quad (8)$$

- (ii) The  $p$ -th order reduced density matrix in coordinate space is defined by

$$\rho^{(p)}(x'_1, \dots, x'_p|x_1, \dots, x_p; t) = \frac{N!}{(N-p)!} \int dx_{p+1} \dots dx_N \psi^*(x'_1, \dots, x'_p, x_{p+1}, \dots, x_N; t) \psi(x_1, \dots, x_p, x_{p+1}, \dots, x_N; t). \quad (9)$$

Eq.9 can also be expressed through field operators as

$$\rho^{(p)}(x'_1, \dots, x'_p|x_1, \dots, x_p; t) = \langle \psi(t) | \hat{\psi}^\dagger(x'_1) \dots \hat{\psi}^\dagger(x'_p) \hat{\psi}(x_p) \dots \hat{\psi}(x_1) | \psi(t) \rangle \quad (10)$$

The diagonal of  $p$ -body density can be represented as

$$\rho^{(p)}(x_1, \dots, x_p; t) = \langle \psi(t) | \hat{\psi}^\dagger(x_1) \dots \hat{\psi}^\dagger(x_p) \hat{\psi}(x_p) \dots \hat{\psi}(x_1) | \psi(t) \rangle \quad (11)$$

It provides the  $p$ -particle density distribution at time  $t$ .

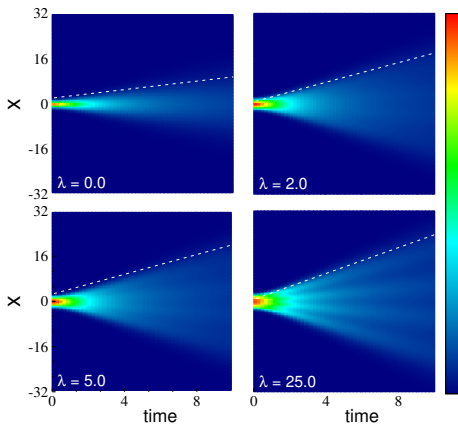


FIG. 1. Time evolution of density profile during expansion of 1D interacting bosons for different choices of interaction strength ( $\lambda = 0, 2, 5$  and  $25$ ).

(iii) Apart from the particle distribution function, it is of great interest to calculate the  $p$ -particle probabilities with the corresponding one-particle probabilities. Thus, the calculation of normalized  $p$ -th order Glauber correlation function would be the most important quantity to measure the spatial coherence. It is defined as

$$g^{(p)}(x'_1, \dots, x'_p, x_1, \dots, x_p; t) = \frac{\rho^{(p)}(x_1, \dots, x_p | x'_1, \dots, x'_p; t)}{\sqrt{\prod_{i=1}^p \rho^{(1)}(x_i | x_i; t) \rho^{(1)}(x'_i | x'_i; t)}} \quad (12)$$

The diagonal of  $g^{(p)}(x'_1, \dots, x'_p, x_1, \dots, x_p; t)$  gives a measure of  $p$ -th order coherence and is calculated as

$$g^{(p)}(x_1, \dots, x_p; t) = \frac{\rho^{(p)}(x_1, \dots, x_p; t)}{\prod_{i=1}^p |\rho^{(1)}(x_i)|} \quad (13)$$

If  $|g^{(p)}(x_1, \dots, x_p; t)| = 1$ , the system is fully coherent, otherwise the state is only partially coherent. When  $g^{(p)}(x_1, \dots, x_p; t) > 1$ , the detection probabilities at positions  $x_1, \dots, x_p$  are correlated and  $g^{(p)}(x_1, \dots, x_p; t) < 1$  are anti-correlated. Eq.13 is further utilized to calculate the local two-particle correlation  $g^{(2)}(0, 0)$  and local three-particle correlation  $g^{(3)}(0, 0, 0)$ .

## IV. RESULTS FOR CONTACT INTERACTION

### A. Expansion dynamics

We perform calculation in one special dimension for  $N = 4$  repulsively interacting bosons trapped in an external harmonic oscillator potential well  $V(x) = \frac{1}{2}x^2$ . We do the numerical calculation with the 64 grid in the domain of  $x_{min} = -32$  to  $x_{max} = +32$  and obtain the time-dependent density distribution. For present calculation, we choose interaction strength starting from non-interacting limit to very-strong interaction limit.  $\lambda = 0$

is the non-interacting case, where initially the density is clustered at the centre of the trap. Up to  $\lambda < 5$  belongs to weak interaction class when the density is also clustered at the centre of the trap similar to non-interacting case, however, now it becomes more flatter and broader.  $\lambda = 5$  and  $\lambda = 10$  belong to strong repulsion regime when the density acquires significant modulation.  $\lambda = 25$  is close to fermionized limit, the number of humps saturates to the number of bosons in the system. The bosons start to become fermionized as the total energy and the density becomes very close to the energy and density of four non-interacting spinless fermions. However this is not TG limit which belongs to the integrable class as the total energy of the four interacting bosons is 7.9 which is slightly less than the required energy of 8.0. In order to precisely approach the TG limit, it is necessary to use a large number of orbitals, which is not achievable with our current computation facility. In Fig. 1, we present expansion dynamics for four choices of  $\lambda$ . In the non-interacting case, the density initially clustered at the centre, expands ballistically as expected. For weak interaction ( $\lambda = 2$ ), we observe *close* to ballistic spreading immediately after the gas is released from the trap, whereas at long time it is *truly* ballistic as the gas becomes extremely dilute and the interaction does not play any significant role. Now the spreading is also faster as compared to non-interacting case due to repulsive interaction. One can follow the white dashed line of Fig 1. In strong interaction strength ( $\lambda = 5.0$ ), just after release, when the density of the cloud is almost same the initial density we observe deviation from the ballistic flow which again follows the true ballistic behaviour at longer time. For  $\lambda = 25.0$ , even at  $t = 0$ , we observe prominent effect of strong repulsion at the centre of the trap, the density is already four-fold splitted. On release from the trap, we observe the propagation of four intense jets. However, the expansion of the whole cloud can be distinguished from the expansion of four humps as their spreading dynamics belongs to different time scale, discussed in Fig. 3. In Fig. 2, we plot the one-body density  $\rho(x)$  for  $\lambda = 25$  at different time. We observe that, at  $t = 0$ , the effect of mutual repulsion plays dominating role and four discrete, closely spaced peaks quantify the existence of four strongly repelled bosons. However, the splitting is localized at the centre of the trap due to the effect of the harmonic potential. The inner peaks are prominent, the outermost peaks are less pronounced. After switching off the trap, we monitor the spreading of two innermost peaks separation, two outermost peaks separation as well as expansion of the whole cloud as a function of time. We observe that peaks start to separate as well as additional tail part is developed. With time, the peaks become flattened and the tail part becomes broader. To quantify the spreading of density, we define three different expansion radius:  $R_{ic}(t)$  (expansion radius of the inner core comprising of two innermost peak) is calculated from the separation of two innermost peaks at individual time,  $R_{oc}(t)$  (expansion radius of the outer core comprising of two outermost

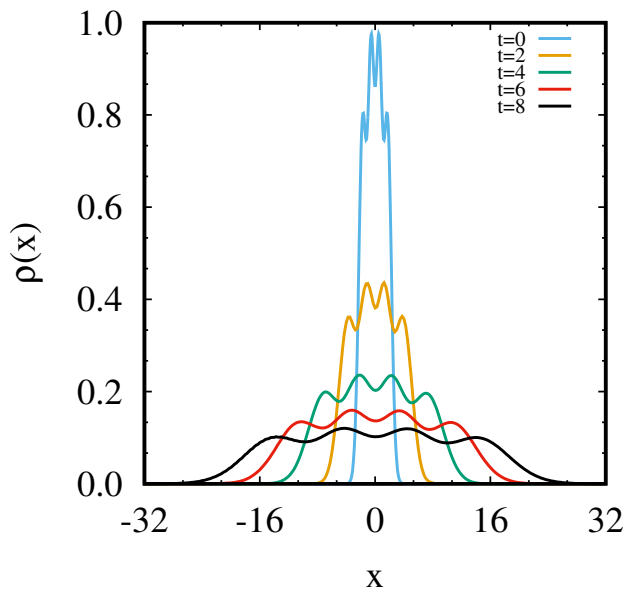


FIG. 2. Plot of one-body density at different times for  $\lambda = 25$ . Initially, all particles are confined at the centre of the harmonic oscillator potential with distinct feature of four peaks corresponding to four strongly interacting bosons. Bosons begin to spread upon trap release. The peak of the cloud shrink and the width expands as expected. See the text for details.

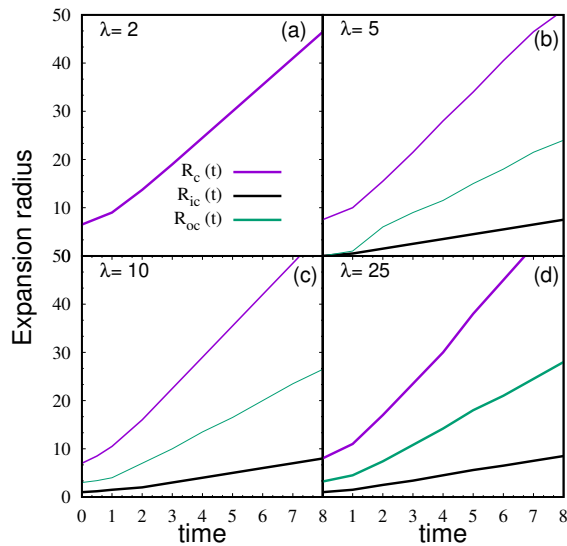


FIG. 3. Expansion radius is plotted as a function of time for different choices of interaction strength.  $R_{ic}(t)$  corresponds to separation of two innermost peaks,  $R_{oc}(t)$  corresponds to separation of two outermost peaks and  $R_c(t)$  is the rms radius of the whole cloud. For weak interaction ( $\lambda = 2$ ), only  $R_c(t)$  exists and the expansion is unimodal. For strong to very strong interaction, the expansion dynamics is trimodal with three different time scale.

peak) is calculated from the separation of two outermost peaks at individual time, and  $R_c(t)$  (expansion radius of the whole cloud) is the root mean square radius and can be calculated as  $R_c(t) = \sqrt{\int x^2 \rho(x) dx}$ . In Fig. 3, we plot the expansion of the three different radius for different choices of interaction strength. Fig 3 (a), corresponds to  $\lambda = 2$ , when the bosons are initially clustered at the centre of the trap and on switching off the trap, they expand as a whole. There is no distinguished structure of either inner core or outer core. So,  $R_c(t)$  is the only physically measured quantity. In Fig. 3 (b,c,d), we plot the expansion radius for  $\lambda = 5, 10, 25$  respectively, which consider strong to very strong interaction regime. We distinctly observe that the expansion dynamics can be characterised by  $R_{ic}(t)$ ,  $R_{oc}(t)$  and  $R_c(t)$ . As discussed in connection of Fig. 1, we observe deviation from ballistic behaviour for the outer core expansion as well as in the expansion of the whole cloud, till time  $t \simeq 1$ , at later time they linearly increase with time. However the inner core spreading is truly ballistic all throughout and independent of interaction strength. It leads to conclusion that interaction affects the separation of the outermost core as well as the whole cloud. The three expansion radii follow different time-scale of dynamics and we conclude that the expansion dynamics in this regime is *trimodal*.

From the display of three different kinds of expansion radius in Fig. 3, we can allocate a corresponding velocity for each spreading independently. We observe for all interaction regime, at very short time, the radius deviates from  $R \sim t$ . It is justified as just after release the density of the cloud is comparable to the initial density and the interaction plays an important role. However for  $t \geq 1$ , when the cloud becomes dilute, we observe  $R \sim t$  for three different radii and we can associate the corresponding expansion velocity as  $\frac{dR(t)}{dt} = V_{ex}$ . In Fig. 4, we plot the corresponding expansion velocity  $V_{ex}$  as a function of interaction strength  $\lambda$ . This plot demonstrates that there are three distinct types of velocities ( $V_{ex}^{ic}$ ,  $V_{ex}^{oc}$  and  $V_{ex}^c$ ) corresponding to the three independent expansions. Up to  $\lambda = 5$ , as the cloud does not have any internal structure (inner or outer peaks) and the cloud expands as a whole, only  $V_{ex}^c$  exists. The velocity of the cloud  $V_{ex}^c$  (magenta) initially increases with  $\lambda$  as expected and then saturates due to bound nature of the contact interaction. In the strong interaction limit  $\lambda \geq 5$ , the structure in one-body density begins to develop. Thus, from the strong to very strong interaction limit, the velocity of the outer-core  $V_{ex}^{oc}$  (blue) and the velocity of the inner-core  $V_{ex}^{ic}$  (yellow) are computed. Both  $V_{ex}^{ic}$  and  $V_{ex}^{oc}$  saturate with increase in interaction strength as the bound nature of contact interaction. Thus, Fig. 4 clearly exhibits the trimodal expansion dynamics in the regime  $\lambda = 5$  to  $\lambda = 25$  which basically corresponds to strong to very strong interaction whereas for  $\lambda \leq 5$  the dynamics is unimodal.

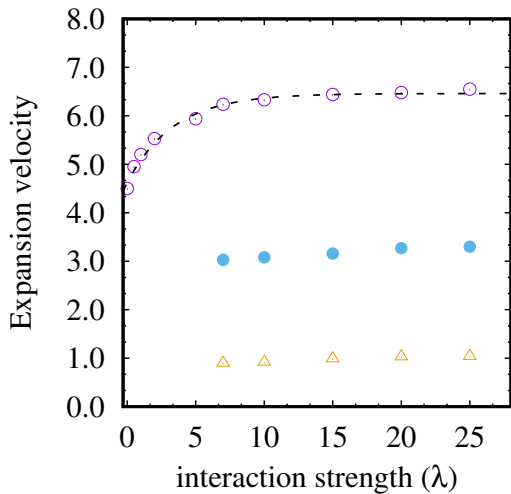


FIG. 4. Expansion velocities  $V_{ex}^{ic}$  (yellow),  $V_{ex}^{oc}$  (blue) and  $V_{ex}^c$  (magenta) as a function of interaction strength. All three velocities saturates with increase in interaction strength. See text for further details.

### B. Dynamics of higher-order density

In this section, We report the expansion dynamics of different higher order densities: two-body density  $\rho^{(2)}(x_1, x_2)$  and three-body density  $\rho^{(3)}(x_1, x_2, x_3 = \text{fixed})$ . The two-body density quantitatively detect the probability to find one particle at  $x_1$  and another at  $x_2$ . Whereas the three-body density  $\rho^{(3)}(x_1, x_2, x_3 = \text{fixed})$  provides the three-body detection probability when the third particle is fixed at some chosen reference point. In Fig. 5, we plot the two- and three-body density for non-interacting bosons. In non-interacting case, all four bosons are initially clustered at the centre ( $x_1 = x_2 = 0$ ) and then propagate uniformly. The higher body density for strong interaction ( $\lambda = 25$ ) is plotted in Fig. 6, the remarkable feature is the development of correlation hole along the diagonal in the two-body density. The correlation hole is defined as  $\rho^{(2)}(x_1, x_2) \rightarrow 0$ , *i.e.*, the probability of finding two bosons at the same position tends to be zero. At such strong interaction strength, the bosons repel each other which leads to fermionization. Thus the correlation hole is the manifestation of Pauli exclusion principle. The bright spots along the sub-diagonal or anti-diagonal ( $x_1 = -x_2$ ) exhibit how the bosons maximise their mutual distance to minimise the potential energy. With time, as the bosons expands, the width of the correlation hole increases and the localized bright spots are also spreaded out. In the three-body density, we fix up the position of the third particle at  $x_3 = 0.0$ . Thus additional correlation hole appears around this fixed point of the third particle which prevent the other bosons to be at these positions.

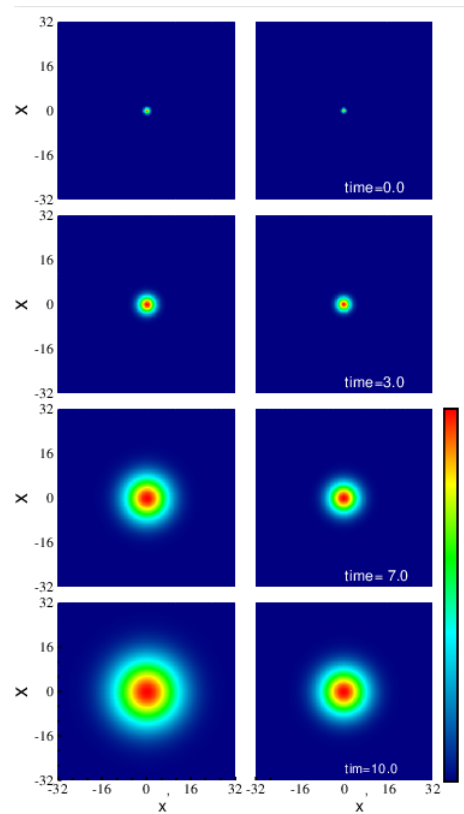


FIG. 5. Snapshot of two-body density  $\rho^{(2)}(x_1, x_2)$  (left column) and three-body density  $\rho^{(3)}(x_1, x_2, x_3 = 0.0)$  (right column) for  $N = 4$  non-interacting bosons at different time.

### C. Correlation dynamics

The diagonal of the  $p$ -th order Glauber correlation function ( $p$ -GC) quantifies the effect of interaction on the measure of coherence of the many-body state. For the non-interacting case, the  $p$ -body density is simply the product of one-body density, the system is fully coherent ( $g^{(p)} = 1$ ) for all time. However, for interacting bosons, the  $p$ -body density is not the product of one-body density and  $g^{(p)} \neq 1$ , implies the system is partially coherent. In Fig. 7, we present the local two-particle correlation  $g^{(2)}(0, 0)$  and local three particle correlation  $g^{(3)}(0, 0, 0)$  as a function of time. These correlation functions measure the probabilities of finding two and three particles at the same place respectively. At  $t = 0$ ,  $g^{(2)}(0, 0)$  is very small but not exactly zero as we belong to the strong interaction regime but not in TG limit. So, exact extinction of two-body correlation is not expected. With time,  $g^{(2)}(0, 0)$  decreases as it would be and it is in good agreement with the expansion of correlation hole discussed in connection with Fig. 6.

We also recognize that  $g^{(3)}(0, 0, 0)$  is insignificant which rules out the possibility of formation of higher order cluster. In Fig 8, We plot the Glauber correlation function  $g^{(2)}(x_1, x_2)$  for  $\lambda = 25$  at different time. They

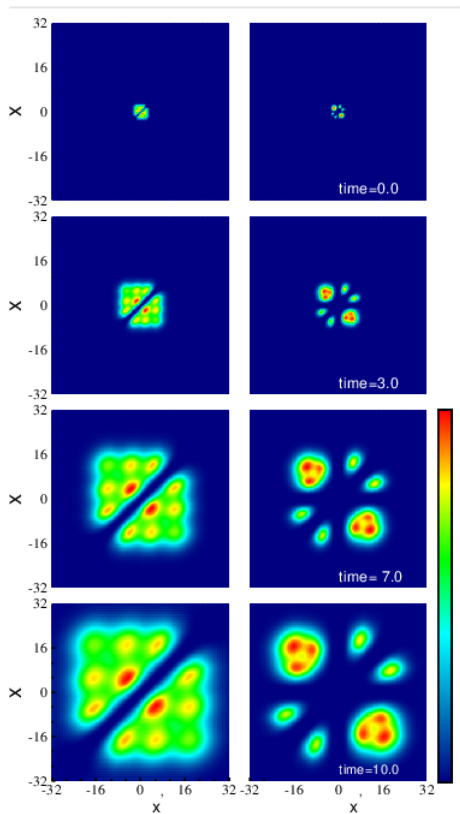


FIG. 6. Snapshot of two-body density  $\rho^{(2)}(x_1, x_2)$  (left column) and three-body density  $\rho^{(3)}(x_1, x_2, x_3 = 0.0)$  (right column) for  $N = 4$  strongly interacting bosons ( $\lambda = 25.0$ ) at different time.

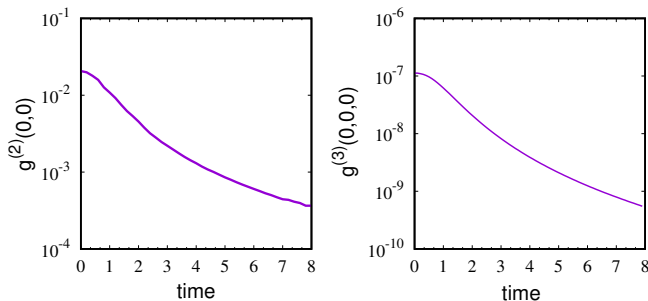


FIG. 7. Two-particle local correlation function  $g^{(2)}(0, 0)$  and three particle local correlation function  $g^{(3)}(0, 0, 0)$  as a function of time for interaction strength  $\lambda = 25.0$ . The decrease of  $g^{(2)}(0, 0)$  over time corresponds to cloud expansion and insignificantly small value of  $g^{(3)}(0, 0, 0)$  rules out the possibility of cluster formation.

are symmetric with respect to the diagonal. Initially second order coherence is maintained except the diagonal ( $x_1 = x_2$ ) and along the diagonal, anti-bunching effect starts to develop. The vanishing diagonal part of normalized two-body correlation function is termed as anti-bunching effect [33]. With time, the off-diagonal correlation is maintained but the anti-bunching effect becomes more prominent.

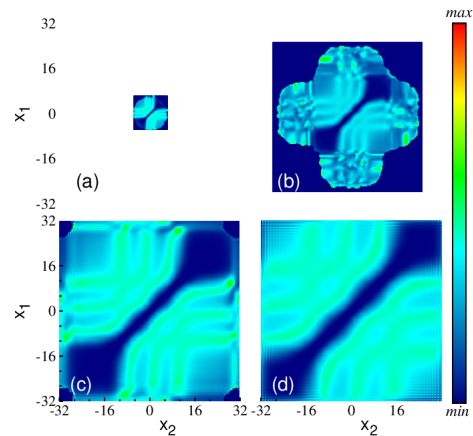


FIG. 8. Snapshot of second-order correlation function  $g^{(2)}(x_1, x_2)$  for  $N = 4$  strongly interacting ( $\lambda = 25$ ) bosons at different time. Antibunching effect and formation of correlation hole along the diagonal are clearly visible.

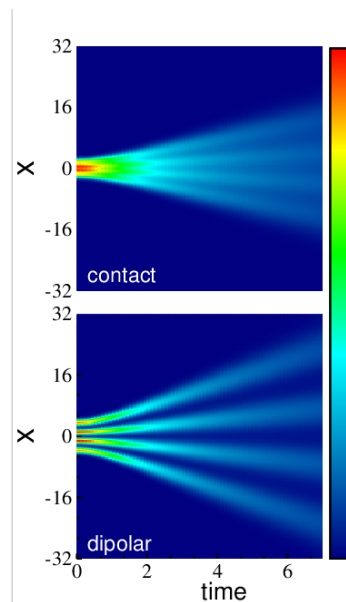


FIG. 9. Time evolution of density profile during expansion of 1D interacting bosons for contact and dipolar interaction strength ( $\lambda = 25$  and  $g_d = 25$ ). See text for full details.

## V. RESULTS FOR DIPOLAR INTERACTION

There is a stringent difference between the short-range contact and long-range dipolar interaction. On increase in interaction strength, the energy is bound for the first case whereas it is unbound in the later case. Thus, very strong interaction in the first case leads to fermionization and the same in the second case leads to crystallization [49]. Due to the repulsive long-range tail of dipolar interaction, the bosons maximally separate with minimize spatial overlap.

To study the consequence of the long-range interaction

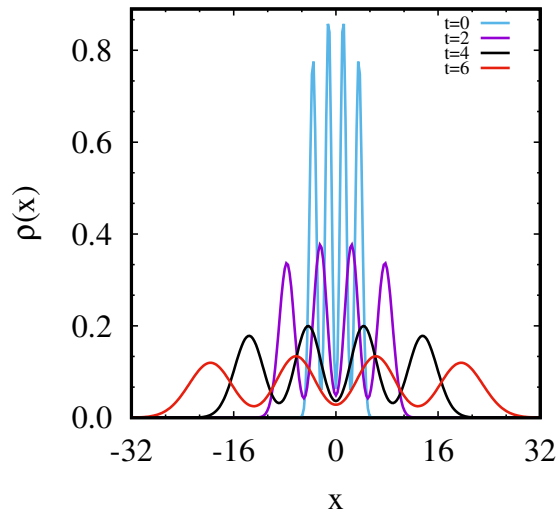


FIG. 10. Plot of one-body density at different times for  $\lambda = 25$ . Initially, all particles are confined at the centre of the harmonic oscillator potential with distinct feature of four peaks corresponding to four strongly interacting bosons. Bosons begin to spread upon trap release. The peak of the cloud shrink and the width expands as expected. The peaks here are more prominent compare to short-range interaction (see Fig. 2).

in the expansion dynamics, we follow the similar kind of analysis that we did for contact interaction. We prepare the  $1D$  trapped dipolar bosons in ground state in the harmonic oscillator potential and suddenly remove the trap, monitor the expansion dynamics. We summarize our numerical results in Fig. 9, Fig. 10 and Fig. 11. In Fig. 9, we plot the spreading of density for dipolar interaction and compare it with the contact interaction for the strong interaction with strength parameter ( $\lambda = g_d = 25$ ). For dipolar interaction, even at  $t = 0$ , four well-isolated peaks are observed, in contrast with the case of contact interaction, where the peaks are localized. Immediately releasing from the trap ( $t > 0$ ), we find a very fast expansion of four bright coloured jets in the case of dipolar interaction. The jets are now more distinct compared to contact interaction. The expansion clearly exhibits diverging nature whereas the same for contact interaction is less divergent. We conclude that the unbounded spreading of density for dipolar interaction is the consequences of unbound energy as  $g_d$  goes to very high value.

To get more insight of the expansion dynamics, we plot one-body density at different times for  $g_d = 25$  in Fig. 10. Comparing with the Fig. 2 (the same for contact interaction), we observe that the width of the density profile rapidly spreaded out for dipolar interaction. The peaks are now well isolated and four-fold splitting is complete. Whereas in Fig. 2, we find four peaks are not isolated and four-fold splitting is incomplete. To quantify the spreading, we further calculate the velocity of the expanding cloud, which is calculated from the spreading of rms radius as described before and plot it in Fig. 11. It is clearly

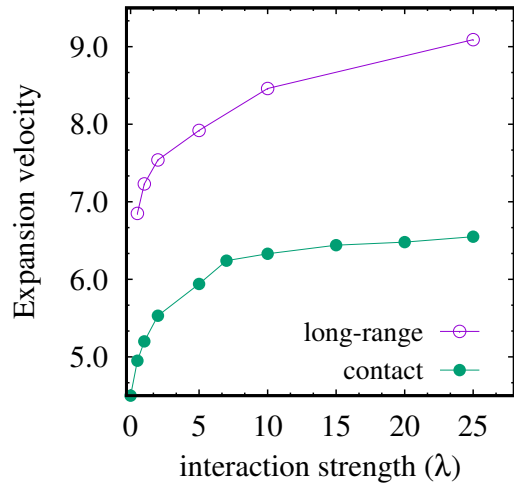


FIG. 11. Expansion velocity of the rms radius ( $V_{ex}^c$ ) for contact interaction (green) and for dipolar interaction (magenta) as a function of strength of interaction.  $V_{ex}^c$  saturates with increase in interaction strength for contact interaction whereas  $V_{ex}^c$  diverges for long-range dipolar interaction. See text for further details.

seen that velocity smoothly saturates for contact interaction whereas it diverges for the dipolar interaction. We have also found (not shown here), that the expansion dynamics is again trimodal as for the case of contact interaction. Thus, we conclude that the expansion dynamics of crystallized bosons is trimodal and unbound with diverging velocity unlike the case of fermionized bosons for which the dynamics is trimodal but bound.

## VI. CONCLUSION

In this paper, we study the expansion dynamics of one dimensional strongly interacting bosons from first principles using the MCTDHB method. It is an established fact that both in the non-interacting limit as well as in TG limit, the expansion is ballistic. Our motivation is to probe the range of interaction, which includes weak to very strong interaction regime close to fermionization limit and beyond the scope of applicability of any integrable model. We observe very complex expansion dynamics in our present calculation. We monitor three different kinds of expansion: expansion of inner-core, expansion of outer-core and full cloud expansion. They are associated with three different time scales and the expansion dynamics is trimodal. Whereas for weak interaction, it is simply unimodal. On increasing in interaction strength, the expansion velocity saturates which confirm that the energy is bounded for contact interaction. We also report the dynamics of higher body density and correlation and recognize the formation of a correlation hole and its spreading with time. To observe the effect of long-range interaction, we do the numerical investigation of expansion dynamics for one-dimensional

dipolar bosons. In the very strong interaction limit, when the short-range contact interaction leads to fermionization, the long range interaction leads to crystallization. We find distinct difference in the expansion dynamics. For contact interaction, we find four-fold splitting (for  $N = 4$  bosons) is incomplete and due to bound nature of the energy, the expansion of the four jets is also bounded. For dipolar interaction, as the energy is unbounded, the four-fold splitting is complete and four jets are now very distinct and spread in unbounded fashion with higher velocity.

## ACKNOWLEDGMENTS

R. R acknowledges the University Grant Commission (UGC) India for the financial support as a senior research fellow. A.G. also acknowledge the Brazilian agencies Fundação de Amparo à Pesquisa do Estado de São Paulo (FAPESP) [Contract 2016/17612-7] and Conselho Nacional de Desenvolvimento Científico e Tecnológico [Procs. 306920/2018-2].

- 
- [1] I. Bloch, J. Dalibard, W. Zwerger, *Rev. Mod. Phys.* **80**, 885 (2008)
- [2] A. Polkovnikov, K. Sengupta, A. Silva, M. Vengalattore, *Rev. Mod. Phys.* **83**, 863 (2011)
- [3] A. Görlitz, J.M. Vogels, A.E. Leanhardt, C. Raman, T.L. Gustavson, J.R. Abo-Shaeer, A.P. Chikkatur, S. Gupta, S. Inouye, T. Rosenband, W. Ketterle, *Phys. Rev. Lett.* **87**, 130402 (2001)
- [4] F. Schreck, L. Khaykovich, K.L. Corwin, G. Ferrari, T. Bourdel, J. Cubizolles, C. Salomon, *Phys. Rev. Lett.* **87**, 080403 (2001)
- [5] M. Greiner, I. Bloch, O. Mandel, T.W. Hänsch, T. Esslinger, *Phys. Rev. Lett.* **87**, 160405 (2001)
- [6] C. Chin, R. Grimm, P. Julienne, E. Tiesinga, *Rev. Mod. Phys.* **82**, 1225 (2010)
- [7] K. Henderson, C. Ryu, C. MacCormick, M.G. Boshier, *New Journal of Physics* **11**(4), 043030 (2009)
- [8] M. Rigol, V. Dunjko, M. Olshanii, *Nature* **452**(7189), 854 (2008)
- [9] N. Sedlmayr, J. Ren, F. Gebhard, J. Sirker, *Phys. Rev. Lett.* **110**, 100406 (2013)
- [10] G. Markus, M. Olaf, H. Theodor W., I. Bloch, *Nature* **419**, 51 (2002)
- [11] S. Trotzky, Y.A. Chen, A. Flesch, I.P. McCulloch, U. Schollwöck, J. Eisert, I. Bloch, *Nature Physics* **8**(4), 325 (2012)
- [12] T. Kinoshita, T. Wenger, D.S. Weiss, *Nature* **440**(7086), 900 (2006)
- [13] N. Strohmaier, Y. Takasu, K. Günter, R. Jördens, M. Köhl, H. Moritz, T. Esslinger, *Phys. Rev. Lett.* **99**, 220601 (2007)
- [14] J.P. Brantut, J. Meineke, D. Stadler, S. Krinner, T. Esslinger, *Science* **337**(6098), 1069 (2012)
- [15] U. Schneider, L. Hackermüller, J.P. Ronzheimer, S. Will, S. Braun, T. Best, I. Bloch, E. Demler, S. Mandt, D. Rasch, A. Rosch, *Nature Physics* **8**(3), 213 (2012)
- [16] I. Gotlibovych, T.F. Schmidutz, A.L. Gaunt, N. Navon, R.P. Smith, Z. Hadzibabic, *Phys. Rev. A* **89**, 061604 (2014)
- [17] O. Morsch, M. Cristiani, J.H. Müller, D. Ciampini, E. Arimondo, *Phys. Rev. A* **66**, 021601 (2002)
- [18] J.P. Ronzheimer, M. Schreiber, S. Braun, S.S. Hodgman, S. Langer, I.P. McCulloch, F. Heidrich-Meisner, I. Bloch, U. Schneider, *Phys. Rev. Lett.* **110**, 205301 (2013)
- [19] S. Langer, M.J.A. Schuetz, I.P. McCulloch, U. Schollwöck, F. Heidrich-Meisner, *Phys. Rev. A* **85**, 043618 (2012)
- [20] T. Kinoshita, T. Wenger, D.S. Weiss, *Science* **305**(5687), 1125 (2004)
- [21] M. Rigol, A. Muramatsu, *Phys. Rev. A* **70**, 031603 (2004)
- [22] M. Rigol, A. Muramatsu, *Phys. Rev. Lett.* **93**, 230404 (2004)
- [23] S. Bera, R. Roy, B. Chakrabarti, *AIP Conference Proceedings* **2072**(1), 020011 (2019)
- [24] S. Langer, F. Heidrich-Meisner, J. Gemmer, I.P. McCulloch, U. Schollwöck, *Phys. Rev. B* **79**, 214409 (2009)
- [25] C.D.E. Boschi, E. Ercolessi, L. Ferrari, P. Naldesi, F. Ortolani, L. Taddia, *Phys. Rev. A* **90**, 043606 (2014)
- [26] J. Ren, Y.Z. Wu, X.F. Xu, *Scientific Reports* **5**(1), 14743 (2015)
- [27] U.R. Fischer, A.U.J. Lode, B. Chatterjee, *Phys. Rev. A* **91**, 063621 (2015)
- [28] A. Browaeys, D. Barredo, T. Lahaye, *Journal of Physics B: Atomic, Molecular and Optical Physics* **49**(15), 152001 (2016)
- [29] M.F. Andersen, *Advances in Physics: X* **7**(1), 2064231 (2022)
- [30] A. Fuhrmanek, A.M. Lance, C. Tuchendler, P. Grangier, Y.R.P. Sortais, A. Browaeys, *New Journal of Physics* **12**(5), 053028 (2010)
- [31] H. Ott, *Reports on Progress in Physics* **79**(5), 054401 (2016)
- [32] O.E. Alon, A.I. Streltsov, L.S. Cederbaum, *Phys. Rev. A* **77**, 033613 (2008)
- [33] R. Roy, A. Gammal, M.C. Tsatsos, B. Chatterjee, B. Chakrabarti, A.U.J. Lode, *Phys. Rev. A* **97**, 043625 (2018)
- [34] O.E. Alon, A.I. Streltsov, L.S. Cederbaum, *Phys. Rev. A* **76**, 062501 (2007)
- [35] Q. Beaufils, R. Chicireanu, T. Zanon, B. Laburthe-Tolra, E. Maréchal, L. Vernac, J.C. Keller, O. Gorceix, *Phys. Rev. A* **77**, 061601 (2008)
- [36] A.S. Arkhipov, G.E. Astrakharchik, A.V. Belikov, Y.E. Lozovik, *Journal of Experimental and Theoretical Physics Letters* **82**(1), 39 (2005)
- [37] F. Deuretzbacher, J.C. Cremon, S.M. Reimann, *Phys. Rev. A* **81**, 063616 (2010)
- [38] P. Košćik, *Physics Letters A* **379**(4), 293 (2015)
- [39] S. Zöllner, *Phys. Rev. A* **84**, 063619 (2011)
- [40] G.E. Astrakharchik, G. Morigi, G. De Chiara, J. Boronat, *Phys. Rev. A* **78**, 063622 (2008)
- [41] B. Chatterjee, A.U.J. Lode, *Phys. Rev. A* **98**, 053624 (2018)
- [42] B. Chatterjee, I. Brouzos, L. Cao, P. Schmelcher, *Journal of Physics B: Atomic, Molecular and Optical Physics*

- 46**(8), 085304 (2013)
- [43] L. Santos, G.V. Shlyapnikov, M. Lewenstein, Phys. Rev. Lett. **90**, 250403 (2003)
- [44] A. André, D. DeMille, J.M. Doyle, M.D. Lukin, S.E. Maxwell, P. Rabl, R.J. Schoelkopf, P. Zoller, Nature Physics **2**(9), 636 (2006)
- [45] H.P. Büchler, E. Demler, M. Lukin, A. Micheli, N. Prokof'ev, G. Pupillo, P. Zoller, Phys. Rev. Lett. **98**, 060404 (2007)
- [46] M. Baranov, Physics Reports **464**(3), 71 (2008)
- [47] A. Griesmaier, J. Werner, S. Hensler, J. Stuhler, T. Pfau, Phys. Rev. Lett. **94**, 160401 (2005)
- [48] P. Mognini, C. Lévêque, H. Keßler, D. Jaksch, R. Chitra, A.U.J. Lode, Phys. Rev. A **106**, L011701 (2022)
- [49] S. Bera, B. Chakrabarti, A. Gammal, M.C. Tsatsos, M.L. Lekala, B. Chatterjee, C. Lévêque, A.U.J. Lode, Scientific Reports **9**(1), 17873 (2019)
- [50] R. Lin, P. Mognini, L. Papariello, M.C. Tsatsos, C. Lévêque, S.E. Weiner, E. Fasshauer, R. Chitra, A.U.J. Lode, Quantum Science and Technology **5**(2), 024004 (2020)
- [51] A.U.J. Lode, Phys. Rev. A **93**, 063601 (2016)
- [52] A.U.J. Lode, C. Lévêque, L.B. Madsen, A.I. Streltsov, O.E. Alon, Rev. Mod. Phys. **92**, 011001 (2020)
- [53] R. Lin, C. Georges, J. Klinder, P. Mognini, M. Büttner, A.U.J. Lode, R. Chitra, A. Hemmerich, H. Keßler, SciPost Phys. **11**, 30 (2021)
- [54] J.H.V. Nguyen, M.C. Tsatsos, D. Luo, A.U.J. Lode, G.D. Telles, V.S. Bagnato, R.G. Hulet, Phys. Rev. X **9**, 011052 (2019)
- [55] O.E. Alon, A.I. Streltsov, L.S. Cederbaum, The Journal of Chemical Physics **127**(15), 154103 (2007)
- [56] A.U.J. Lode, K. Sakmann, O.E. Alon, L.S. Cederbaum, A.I. Streltsov, Phys. Rev. A **86**, 063606 (2012)
- [57] A.U.J. Lode, B. Chakrabarti, V.K.B. Kota, Phys. Rev. A **92**, 033622 (2015)
- [58] R. Roy, C. Lévêque, A.U.J. Lode, A. Gammal, B. Chakrabarti, Quantum Reports **1**(2), 304 (2019)
- [59] R. Roy, B. Chakrabarti, A. Trombettoni, European Physical Journal D **76**(24), 215303 (2022)
- [60] A.I. Streltsov, O.E. Alon, L.S. Cederbaum, Phys. Rev. Lett. **99**, 030402 (2007)
- [61] E. Fasshauer, A.U.J. Lode, Phys. Rev. A **93**, 033635 (2016)
- [62] A.U.J. Lode, C. Bruder, Phys. Rev. A **94**, 013616 (2016)
- [63] A.U.J. Lode, M.C. Tsatsos, E. Fasshauer, S.E. Weiner, R. Lin, L. Papariello, P. Mognini, C. Lévêque, M. Büttner, J. Xiang, S. Dutta, MCTDH-X: The MultiConfigurational Time-Dependent Hartree Method for Indistinguishable Particles Software (2022)
- [64] S. Kvaal, Molecular Physics **111**(9-11), 1100 (2013)
- [65] P. Kramer, M. Saraceno, *Geometry of the Time-Dependent Variational Principle in Quantum Mechanics* (Springer Berlin, Heidelberg, 1981)
- [66] A. McLachlan, Molecular Physics **8**(1), 39 (1964)
- [67] L. Cao, V. Bolsinger, S.I. Mistakidis, G.M. Koutentakis, S. Krönke, J.M. Schurer, P. Schmelcher, J. Chem. Phys. **147**, 044106 (2017)
- [68] Y. Cai, M. Rosenkranz, Z. Lei, W. Bao, Phys. Rev. A **82**, 043623 (2010)